

# Langevin Dynamics in Constant Pressure Extended Systems

D Quigley\* and MIJ Probert†

University of York

Heslington

York

United Kingdom

YO10 5DD

(Dated: February 8, 2020)

The advantages of performing Langevin Dynamics in extended systems are discussed. A simple Langevin Dynamics scheme for producing the isothermal ensemble is reviewed, and is then extended to the Hoover ensemble. We show that the resulting equations of motion generate the isobaric-isothermal ensemble. The Parrinello-Rahman ensemble is then discussed and we show that despite the presence of intrinsic probability gradients in this system, a Langevin Dynamics approach samples the extended phase space in the correct fashion. The implementation of these methods in the *ab-initio* plane wave density functional theory (DFT) code CASTEP [1] is demonstrated.

PACS numbers: 02.20.Ns 31.15.Qg 33.15.Vb 52.65.Yy 61.20.Ja 83.10.Mj

## I. INTRODUCTION

The method of molecular dynamics is a well established tool with wide ranging applications. Of particular advantage is the ability to obtain ensemble averages of statistical quantities (in ergodic systems) and detailed trajectory information within the same computational framework.

Many of the early attempts to extend molecular dynamics from the micro-canonical (NVE) to the canonical (NVT) ensemble used some form of stochastic dynamics. A random component to the particle dynamics stimulates ergodicity and can reduce correlations for increased sampling efficiency at the expense of accuracy in short-term dynamics. A simple stochastic dynamics scheme based on the Langevin equation will be reviewed in section II.

A more widely adopted scheme for generating NVT ensemble trajectories is the Nosé thermostat [2, 3]. Here time is rescaled according to an extra ‘extended system’ variable. This is introduced to the Hamiltonian in a manner chosen to reproduce the correct NVT partition function and hence simulate coupling to a heat bath. Use of this method requires either a non-uniform sampling in the scaled time variable [2] or a non-canonical transform to un-scaled time [3]. Recent work on non-Hamiltonian statistical mechanics has shown that this is not a major concern for the trajectory of the particle subsystem [4, 5]. Other work has reformulated the Nosé scheme to remove the need for a non-canonical transform [6] altogether.

Of greater concern is the problem of ergodicity. In order to generate correct ensemble averages from MD trajectories, the simulated system *must* be ergodic. The simple deterministic nature of the Nosé scheme requires that the chaotic behaviour needed to stimulate ergodicity is provided by the particle sub-system itself. For certain

systems, in particular those containing harmonic forces, this requirement is known not to be satisfied [3] leading to incorrect phase-space trajectories and hence poor ensemble averages. It is now common practise to overcome this problem by the use of a chain of Nosé-style thermostats [7]. Although guaranteed to correctly sample the isothermal ensemble, this scheme is still deterministic and exhibit longer correlation times than stochastic methods in some circumstances. Note that recent work has generalised the Nosé scheme to include more chaotic terms in the extended Lagrangian [8, 9] which does much to eliminate these issues.

Extended Hamiltonian methods are also available to simulate the coupling of the particle system to a pressure piston. This idea was introduced by Andersen [10] in a scheme where particle positions and momenta are scaled according to the cell volume. Potential and kinetic energy terms for the volume are added to the Lagrangian resulting in an expansion or contraction of the system to regulate pressure with the required fluctuations. A modification of the Andersen scheme in which the extended system variables are the strain rate  $\dot{\epsilon}$  and its conjugate, was introduced by Hoover [11]. This tends to be more robust in practise. A scheme in which the cell motion is anisotropic with each cell vector evolving independently was introduced by Parrinello and Rahman [12, 13].

These constant pressure schemes have been coupled to Nosé style thermostats resulting in schemes for sampling the isobaric-isothermal (NPT) ensemble [14, 15].

Kolb and Dunweg [16] have shown that an effective method for sampling the isobaric-isothermal ensemble can be obtained by performing Langevin dynamics in the extended Andersen system. This has the potential advantage of shorter correlation times and guaranteed ergodicity in the NPT ensemble. In this paper, we show that Langevin dynamics can be conducted within a Hoover-style extended system to correctly sample the isothermal-isobaric ensemble. The extension of these ideas to Langevin dynamics in a Parrinello-Rahman sys-

---

\*Electronic address: dq100@york.ac.uk

†Electronic address: mijpl@york.ac.uk

tem will also be discussed. The resulting equations of motion are integrated using an evolution algorithm obtained from Louville time evolution operators [17] which is symplectic in the limit of zero friction.

Criteria for selecting coupling parameters for the thermostatic/barostatic processes will also be discussed and applied to various example simulations.

## II. LANGEVIN DYNAMICS

A simple but effective method of performing Langevin dynamics simulations for the isothermal ensemble uses the following equations of motion in the usual notation

$$\dot{\mathbf{r}}_i = \mathbf{p}_i/m_i \quad (1a)$$

$$\dot{\mathbf{p}}_i = \mathbf{f}_i - \gamma \mathbf{p}_i + \mathbf{R}_i. \quad (1b)$$

Here  $\gamma$  is a friction co-efficient representing viscous damping due to fictitious ‘heat bath’ particles. The random force  $\mathbf{R}_i$  represents the effect of collisions with these particles. Following Chandrasekhar [18] we assume that the timescale of the collisional heat bath process is very much smaller than the ionic motions of interest, and hence

$$\langle \mathbf{R}_i(t) \mathbf{R}_i(t') \rangle = \delta(t - t'). \quad (2)$$

Furthermore, we assume that a great many collisions with heat bath particles occur over a MD time-step and we can therefore expect that  $\mathbf{R}_i$  will be distributed in a Gaussian fashion in accordance with the central limit theorem. The Stokes-Einstein relation for the diffusion coefficient can then be used to show that the average value of  $\mathbf{R}_i$  over a time-step (in thermal equilibrium) should be a random deviate drawn from a Gaussian distribution of zero mean and unit variance scaled by

$$\sqrt{\frac{2k_B T \gamma m}{\Delta t}}. \quad (3)$$

Note that this choice of  $\mathbf{R}_i$  limits this simple scheme, and the constant pressure schemes that follow, to equilibrium simulations only. Certain deterministic thermostats can however be utilised in non-equilibrium simulations [19].

It can be shown that equations 1a and 1b are equivalent to the following Fokker-Planck equation for the phase space probability density  $\rho(\mathbf{r}^N, \mathbf{p}^N)$

$$\begin{aligned} \frac{\partial}{\partial t} \rho + \sum_{i=1}^N \left[ \frac{\mathbf{p}_i}{m} \cdot \nabla_{\mathbf{r}_i} \rho + \mathbf{f}_i \cdot \nabla_{\mathbf{p}_i} \rho \right] \\ = \gamma \sum_{i=1}^N \nabla_{\mathbf{p}_i} \cdot [\mathbf{p}_i \rho + m k_B T \nabla_{\mathbf{p}_i} \rho]. \end{aligned} \quad (4)$$

This has the canonical phase space probability density function  $\rho_{NVT}$  as a stationary solution, and hence the method can be used to sample the isothermal ensemble via a fluctuation-dissipation process [20].

The choice of the parameter  $\gamma$  is a compromise between statistical sampling efficiency and preservation of accuracy in short-term dynamics. However, in the case where the process approximated by the stochastic components can be simulated by another method, it is possible to determine an optimal value of  $\gamma$  numerically. Guidelines for the choice of  $\gamma$  will be discussed in detail later.

An effective Verlet-style integrator can be obtained for this scheme by applying the time-evolution operator formulation of Tuckerman *et al* [17] in the limit  $\gamma \rightarrow 0$ . The lack of a Louville operator for the stochastic components of the dynamics requires that these are then included into the particle forces via the following substitutions:

$$\begin{aligned} \mathbf{f}_i(t) &\rightarrow \mathbf{f}_i(t) - \gamma \mathbf{p}_i(t) + \mathbf{R}_i(t) \\ \mathbf{f}_i(t + \Delta t) &\rightarrow \mathbf{f}_i(t + \Delta t) - \gamma \mathbf{p}_i(t + \Delta t) + \mathbf{R}_i(t + \Delta t) \end{aligned}$$

In the NVT case described here, this leads to standard Velocity-Verlet, modified with the above substitutions.

## III. LANGEVIN-HOOVER DYNAMICS

In this section, we show that the simple NVT scheme above can be extended to perform Langevin dynamics in a Hoover-style extended system, and that this results in correct sampling of the isobaric-isothermal ensemble.

### A. Equations of Motion

The equations of motion we propose are shown below. These incorporate the constant pressure component of the Hoover equations as corrected by Martyna *et al* [14]. In the form shown below, the deterministic equations for the evolution of both the particle and barostat velocity have been converted to Langevin equations in  $d$  dimensions with different friction constants

$$\dot{\mathbf{r}}_i = \frac{\mathbf{p}_i}{m_i} + \frac{p_\epsilon}{W} \mathbf{r}_i \quad (5a)$$

$$\dot{\mathbf{p}}_i = -\nabla_{\mathbf{r}_i} \Phi - \left(1 + \frac{d}{N_f}\right) \frac{p_\epsilon}{W} \mathbf{p}_i - \gamma \mathbf{p}_i + \mathbf{R}_i \quad (5b)$$

$$\dot{\mathcal{V}} = d \mathcal{V} p_\epsilon / W \quad (5c)$$

$$\dot{p}_\epsilon = d \mathcal{V} (X - P_{ext}) + \frac{d}{N_f} \sum_{i=1}^N \frac{\mathbf{p}_i^2}{m_i} - \gamma_p p_\epsilon + R_p. \quad (5d)$$

These equations introduce the volume  $\mathcal{V}$  as a dynamical (barostat) variable. The corresponding momentum variable  $p_\epsilon$  is the strain rate  $\dot{\epsilon}$  multiplied by a fictitious mass  $W$ .  $R_p$  is a stochastic ‘force’ which acts on the barostat. The use of a Langevin equation for the barostat as

well as the particles may have possible equilibration benefits, but we shall see in the analysis that follows that it is not required for canonical sampling at equilibrium.

The scalar  $X$  is given by

$$X = \frac{1}{dV} \left[ \sum_{i=1}^N \frac{\mathbf{p}_i \cdot \mathbf{p}_i}{m_i} + \sum_{i=1}^N \mathbf{r}_i \cdot \mathbf{f}_i \right] - \frac{\partial}{\partial V} \Phi(\mathbf{r}^N, \mathcal{V}). \quad (6)$$

The distinction between  $X$  and the instantaneous pressure  $\mathcal{P}$  is important. The value of  $\mathcal{P}$  when calculated using the virial equation should include the white noise contributions from the ‘Langevin thermostat’ whereas  $X$  does not. Use of  $\mathcal{P}$  in equation 5d leads to non-canonical temperature and volume fluctuations.

The values of  $\mathbf{R}_i$  are drawn from the same distribution as the NVT case. Values of  $R_p$  are drawn from a Gaussian distribution of zero mean and unit variance scaled by

$$\sqrt{\frac{2k_B W \gamma_p}{\Delta t}}. \quad (7)$$

In the un-thermostatted limit ( $\gamma \rightarrow 0, \gamma_p \rightarrow 0$ ) equations 5a to 5b obey the Liouville theorem

$$\frac{\partial \rho}{\partial t} + \sum_{i=1}^N \dot{\mathbf{r}}_i \cdot \nabla_{\mathbf{r}_i} \rho + \sum_{i=1}^N \dot{\mathbf{p}}_i \cdot \nabla_{\mathbf{p}_i} \rho + \dot{p}_\epsilon \frac{\partial \rho}{\partial p_\epsilon} + \dot{\mathcal{V}} \frac{\partial \rho}{\partial \mathcal{V}} = 0 \quad (8)$$

and conserve the quantity

$$H' = \mathcal{H}(\mathbf{r}^N, \mathbf{p}^N) + P\mathcal{V} + p_\epsilon^2/2W, \quad (9)$$

where  $\mathcal{H}$  is the Hamiltonian of the particle sub-system. Note that  $H'$  itself is not a Hamiltonian. A rigorous phase space analysis is therefore best performed using techniques in non-Hamiltonian statistical mechanics as introduced by Tuckerman and co-workers [4, 5].

## B. Justification

To show that equations 5a to 5d correctly sample the isobaric-isothermal ensemble we first identify the un-thermostatted phase-space probability density for the extended system of particles,

$$\rho_{NPH'}(\mathbf{r}^N, \mathbf{p}^N, p_\epsilon, \mathcal{V}) \propto \frac{\delta[H'(t) - H'(0)]}{\Omega_{NPH'}(\mathbf{r}^N, \mathbf{p}^N, p_\epsilon, \mathcal{V})}. \quad (10)$$

The phase space density for this system coupled to a heat bath at constant temperature should therefore be

$$\rho_{NPT}(\mathbf{r}^N, \mathbf{p}^N, p_\epsilon, \mathcal{V}) \propto \frac{1}{\Omega_{NPT}(\mathbf{r}^N, \mathbf{p}^N, p_\epsilon, \mathcal{V})} \times \exp \left[ -\frac{\mathcal{H}(\mathbf{r}^N, \mathbf{p}^N) + P\mathcal{V} + p_\epsilon^2/2W}{k_B T} \right]. \quad (11)$$

This is the probability density function for the correctly thermostatted extended particle plus barostat phase space. Integration over the barostat momentum  $p_\epsilon$  yields a constant, and hence

$$\rho_{NPT}(\mathbf{r}^N, \mathbf{p}^N, \mathcal{V}) \propto \frac{1}{\Omega_{NPT}(\mathbf{r}^N, \mathbf{p}^N, \mathcal{V})} \times \exp \left[ -\frac{\mathcal{H}(\mathbf{r}^N, \mathbf{p}^N) + P\mathcal{V}}{k_B T} \right]. \quad (12)$$

which is the correct probability density function for the isobaric-isothermal particle subsystem.

Following Stratonovich [21] we now construct the following Fokker-Planck equation for the phase space density  $\rho$  resulting from equations 5a to 5d. The compressibility of equations 5a to 5d is zero and hence the Jacobian of the resulting co-ordinate transform is the identity matrix and we need not include it:

$$\begin{aligned} \frac{\partial \rho}{\partial t} &+ \sum_{i=1}^N \left\{ \left( \frac{\mathbf{p}_i}{m_i} + \frac{p_\epsilon}{W} \mathbf{r}_i \right) \cdot \nabla_{\mathbf{r}_i} \rho + \left[ \mathbf{f}_i - \left( 1 + \frac{d}{N_f} \right) \frac{p_\epsilon}{W} \mathbf{p}_i \right] \cdot \nabla_{\mathbf{p}_i} \rho \right\} \\ &+ \left[ d\mathcal{V}(\chi - P_{ext}) + \frac{d}{N_f} \sum_{i=1}^N \frac{\mathbf{p}_i^2}{m_i} \right] \frac{\partial \rho}{\partial p_\epsilon} + \dot{\mathcal{V}} \frac{\partial \rho}{\partial \mathcal{V}} \\ &= \gamma_p \frac{\partial}{\partial p_\epsilon} \left[ p_\epsilon \rho + W k_B T \frac{\partial}{\partial p_\epsilon} \rho \right] + \gamma \sum_{i=1}^N \nabla_{\mathbf{p}_i} \cdot [\mathbf{p}_i \rho + m k_B T \nabla_{\mathbf{p}_i} \rho]. \end{aligned} \quad (13)$$

where  $\rho = \rho(\mathbf{r}^N, \mathbf{p}^N, p_\epsilon, \mathcal{V})$ .

In order for the Langevin-Hoover scheme to correctly sample the isobaric-isothermal ensemble, equation 11

must be a solution of 13. As the un-thermostatted system is Liouvillian, we expect the LHS of equation 13 to be identically zero which is easily confirmed. Our use of

the Stokes-Einstein relation in balancing the stochastic part of the Langevin dynamics with the dissipative friction term ensures that the RHS is also zero for any phase space probability density function representing equilibrium with a heat bath. This is also easily confirmed in the case where  $\rho$  is given by equation 11, and hence the proposed equations of motion are expected to sample the isobaric-isothermal ensemble in the correct fashion.

A complete justification that the Langevin-Hoover scheme samples the required ensemble must show that the desired temperature and pressure are maintained with canonical fluctuations about the mean of each. This behaviour depends on the choice of the parameters  $W$ ,  $\gamma$  and  $\gamma_p$ , and will be covered in detail in section III D.

### C. Numerical Integration

In this section we follow the method discussed above for obtaining integration algorithms for systems obeying Langevin equations. The Liouville operator for the isotropic Langevin NPT equations of motion in the limit of zero friction is

$$\begin{aligned} iL &= \dot{\mathbf{r}} \frac{\partial}{\partial \mathbf{r}} + \dot{\mathbf{p}} \frac{\partial}{\partial \mathbf{p}} + \dot{\epsilon} \frac{\partial}{\partial \epsilon} + \dot{p}_\epsilon \frac{\partial}{\partial p_\epsilon} \\ &= iL_r + iL_p + iL_\epsilon + iL_{p_\epsilon}. \end{aligned} \quad (14)$$

The following Trotter factorisation of the resulting time-step evolution operators was found to be the most convenient:

$$e^{iL\Delta t} = e^{iL_\epsilon\Delta t/2} e^{iL_{p_\epsilon}\Delta t/2} e^{iL_p\Delta t/2} e^{iL_r\Delta t} \times e^{iL_p\Delta t/2} e^{iL_{p_\epsilon}\Delta t/2} e^{iL_\epsilon\Delta t/2} \quad (15)$$

which leads to the following integration algorithm.

1.  $\mathcal{V}^{t+\frac{1}{2}\Delta t} = \mathcal{V}^t + \frac{\Delta t}{2} \dot{\mathcal{V}}[\mathcal{V}^t, p_\epsilon^t]$
2.  $p_\epsilon^{t+\frac{1}{2}\Delta t} = p_\epsilon^t + \frac{\Delta t}{2} \dot{p}_\epsilon \left[ \mathbf{r}_i^t, \mathbf{p}_i^t, \mathcal{V}^{t+\frac{1}{2}\Delta t}, p_\epsilon^t \right]$
3.  $\mathbf{p}_i^{t+\frac{1}{2}\Delta t} = \mathbf{p}_i^t + \frac{\Delta t}{2} \dot{\mathbf{p}}_i \left[ \mathbf{r}_i^t, \mathbf{p}_i^t, p_\epsilon^{t+\frac{1}{2}\Delta t} \right]$
4.  $\mathbf{r}_i^{t+\Delta t} = \mathbf{r}_i^t + \Delta t \dot{\mathbf{r}}_i \left[ \mathbf{r}_i^t, \mathbf{p}_i^{t+\frac{1}{2}\Delta t}, p_\epsilon^{t+\frac{1}{2}\Delta t} \right]$
5.  $\mathbf{p}_i^{t+\Delta t} = \mathbf{p}_i^{t+\frac{1}{2}\Delta t} + \frac{\Delta t}{2} \dot{\mathbf{p}}_i \left[ \mathbf{r}_i^{t+\Delta t}, \mathbf{p}_i^{t+\frac{1}{2}\Delta t}, p_\epsilon^{t+\frac{1}{2}\Delta t} \right]$
6.  $p_\epsilon^{t+\Delta t} = p_\epsilon^{t+\frac{1}{2}\Delta t} + \frac{\Delta t}{2} \dot{p}_\epsilon \left[ \mathbf{r}_i^{t+\Delta t}, \mathbf{p}_i^{t+\Delta t}, \mathcal{V}^{t+\frac{1}{2}\Delta t}, p_\epsilon^{t+\frac{1}{2}\Delta t} \right]$
7.  $\mathcal{V}^{t+\Delta t} = \mathcal{V}^t + \frac{\Delta t}{2} \dot{\mathcal{V}} \left[ \mathcal{V}^{t+\frac{1}{2}\Delta t}, p_\epsilon^{t+\Delta t} \right].$

Making the appropriate substitution for the particle forces at each time-step we now include the Langevin buffeting and damping terms and denote these as extra dependences of the time derivatives.

1.  $\mathcal{V}^{t+\frac{1}{2}\Delta t} = \mathcal{V}^t + \frac{\Delta t}{2} \dot{\mathcal{V}}[\mathcal{V}^t, p_\epsilon^t]$
2.  $p_\epsilon^{t+\frac{1}{2}\Delta t} = p_\epsilon^t + \frac{\Delta t}{2} \dot{p}_\epsilon \left[ \mathbf{r}_i^t, \mathbf{p}_i^t, \mathcal{V}^{t+\frac{1}{2}\Delta t}, p_\epsilon^t, \gamma_p p_\epsilon^t, R_p^t \right]$
3.  $\mathbf{p}_i^{t+\frac{1}{2}\Delta t} = \mathbf{p}_i^t + \frac{\Delta t}{2} \dot{\mathbf{p}}_i \left[ \mathbf{r}_i^t, \mathbf{p}_i^t, p_\epsilon^{t+\frac{1}{2}\Delta t}, \gamma \mathbf{p}_i^t, \mathbf{R}_i^t \right]$
4.  $\mathbf{r}_i^{t+\Delta t} = \mathbf{r}_i^t + \Delta t \dot{\mathbf{r}}_i \left[ \mathbf{r}_i^t, \mathbf{p}_i^{t+\frac{1}{2}\Delta t}, p_\epsilon^{t+\frac{1}{2}\Delta t} \right]$
5.  $\mathbf{p}_i^{t+\Delta t} = \mathbf{p}_i^{t+\frac{1}{2}\Delta t} + \frac{\Delta t}{2} \dot{\mathbf{p}}_i \left[ \mathbf{r}_i^{t+\Delta t}, \mathbf{p}_i^{t+\frac{1}{2}\Delta t}, p_\epsilon^{t+\frac{1}{2}\Delta t}, \gamma \mathbf{p}_i^{t+\Delta t}, \mathbf{R}_i^{t+\Delta t} \right]$
6.  $p_\epsilon^{t+\Delta t} = p_\epsilon^{t+\frac{1}{2}\Delta t} + \frac{\Delta t}{2} \dot{p}_\epsilon \left[ \mathbf{r}_i^{t+\Delta t}, \mathbf{p}_i^{t+\Delta t}, \mathcal{V}^{t+\frac{1}{2}\Delta t}, p_\epsilon^{t+\Delta t}, \gamma_p p_\epsilon^{t+\Delta t}, R_p^{t+\Delta t} \right]$
7.  $\mathcal{V}^{t+\Delta t} = \mathcal{V}^t + \frac{\Delta t}{2} \dot{\mathcal{V}} \left[ \mathcal{V}^{t+\frac{1}{2}\Delta t}, p_\epsilon^{t+\Delta t} \right].$

To demonstrate the stability of this algorithm we consider the limit of vanishing friction in which  $\gamma \rightarrow 0$ . In this limit the system is Liouvillian and the quantity

$$H' = \Phi(\{\mathbf{r}_i\}) + \sum_{i=1}^N \mathbf{p}_i^2/2m_i + p_\epsilon^2/2W + P_{ext}\mathcal{V} \quad (16)$$

is conserved. Figure 1 shows the value of  $H'$  for a Lennard-Jones system both in the zero friction limit, and for a Langevin-Hoover simulation. With the introduction of finite friction we expect deviations from  $H'$  with no long term drift as indicated.

### D. Choice of Parameters

The isotropic scheme uses three parameters which must be chosen carefully. These are the barostat ‘mass’  $W$ , the particle friction coefficient  $\gamma$  and the barostat friction coefficient  $\gamma_p$ .

It has been previously noted [22] that for a Hoover barostat, the fictitious mass should be chosen according to

$$W = dNk_bT/\omega_b^2 \quad (17)$$

where  $\omega_b$  is the frequency of the required volume fluctuations. The choice of this  $\omega_b$  depends on the timescale

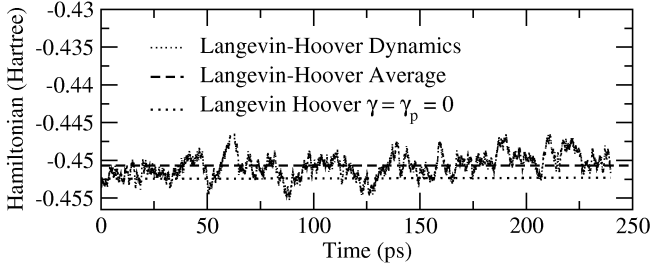


FIG. 1: Value of the conserved quantity in the Hoover system for a Langevin dynamics simulation, and a similar simulation in the zero friction limit. Interactions were modelled with the Lennard-Jones potential for argon at, 67.6 MPa. In the case of the Langevin dynamics simulation, a set temperature of 20 K was used. An equilibration time of 10,000  $\Delta t$  was used prior to sampling. The drift in the zero friction value is less than  $2 \times 10^{-4}$  Hartree over the 100,000 time-step run with  $\Delta t = 2.4$  fs.

on which the particle motions of interest occur. A useful aide when choosing this frequency is the NVT temperature spectrum (TS). The character of this spectrum should not be significantly disrupted by the addition of a barostat. In practise this means choosing  $\omega_b$  to be less than the smallest frequency component in the TS (figure 2). Care must also be taken that  $\omega_b$  is sufficiently close to these components that de-coupling of the barostat from the particle subsystem is avoided.

To determine an appropriate value for the particle friction coefficient  $\gamma$  we calculate the memory function for the system we wish to study. The memory function  $\xi$  for the velocity autocorrelation function  $\psi$  is defined by

$$\frac{d\psi}{dt} = - \int_0^t \xi(t-\tau) \psi(\tau) d\tau. \quad (18)$$

The generalised Langevin equation is

$$\dot{\mathbf{p}}_i = \mathbf{F}_i - \int_0^t \xi(t-\tau) \mathbf{p}_i(\tau) d\tau + \mathbf{R}_i, \quad (19)$$

which in the extended particle + barostat phase space becomes

$$\begin{aligned} \dot{\mathbf{p}}_i = & -\nabla_{\mathbf{r}_i} \Phi - \left(1 + \frac{d}{N_f}\right) \frac{p_\epsilon}{W} \mathbf{p}_i \\ & - \int_0^t \xi(t-\tau) \mathbf{p}_i(\tau) + \mathbf{R}_i. \end{aligned} \quad (20)$$

Comparing to equation 5b, we can see that the stochastic component of the dynamics is generated within the approximation

$$\xi = \gamma \delta(t). \quad (21)$$

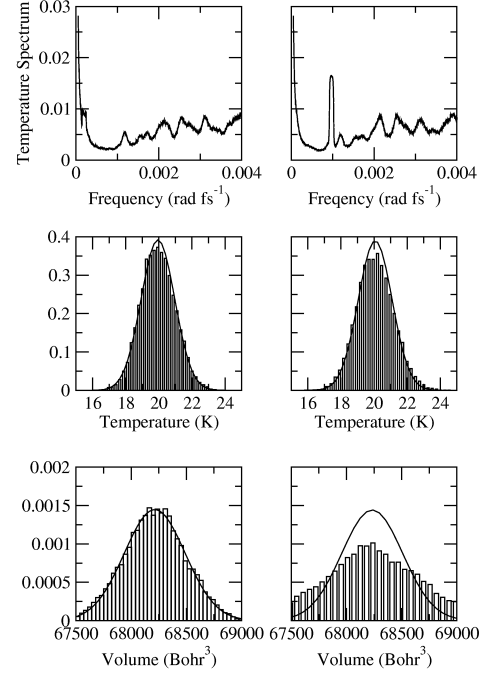


FIG. 2: Choice of  $\omega_b$  for solid Lennard-Jones argon at 50 K 20 MPa. A thermostat frequency  $\omega_p = 2\pi\gamma = 6.6 \times 10^{-4}$  rad fs $^{-1}$  is used in both cases. In the left hand case,  $\omega_b$  is chosen to be less than the lowest frequency which appears in the NVT temperature spectrum. The corresponding temperature and volume sample distributions match the exact canonical (solid line) case exactly. In the right hand case the choice of  $\omega_b$  has disrupted the natural temperature spectrum resulting in non-canonical fluctuations.

To retain consistency with this approximation, the value of gamma should be equal to

$$\gamma = \xi_0 = \int_0^\infty \xi_{act}(\tau) d\tau, \quad (22)$$

where  $\xi_{act}$  is the actual memory function of the system we wish to simulate. Calculation of the optimal  $\gamma$  therefore requires prior knowledge of the memory function which can be obtained from an NVE simulation or from other NVT/NPT techniques. As the stochastic component of the dynamics has now been chosen to be characteristic of the particle motions themselves, the ‘heat bath’ is now representative of the effect of the bulk on our simulated sample. This is particularly appropriate for simulations using periodic boundary conditions, where the only physical objects with which the simulated particles exchange heat, are other particles in neighbouring cells.

A useful method of calculating  $\xi(t)$  from trajectory information via an autoregressive model has been proposed by Kneller and Hinsin [23]. We will use this method to calculate appropriate value of  $\gamma$  for various simple systems in section V A.

The cost of computing a memory function in advance of a Langevin dynamics simulation can sometimes be

prohibitive and it is often convenient to adopt the conservative rule of thumb that the thermostat frequency  $\omega_p = 2\pi/\gamma$  should be a few tens of times smaller than the smallest characteristic frequency of the system to be studied. This may result in less than optimum sampling efficiency, but will generate the NPT ensemble without disrupting the particle motions of interest.

The choice of the ‘piston thermostat’ parameter  $\gamma_p$  is of less importance. The inclusion of the damping and buffeting terms in equation 5d is not necessary for reproduction of the NPT partition function, however a non-zero  $\gamma_p$  may equilibration times. Furthermore the effect on the particle velocities is small in equilibrium. We generally require that  $2\pi/\gamma_p$  be ten times smaller than the frequency associated with the barostat variable. It is in principle possible to calculate an autocorrelation function

for  $p_\epsilon$  and hence a memory function and optimal barostatic friction coefficient. This is not useful in practise.

#### IV. LANGEVIN-PARRINELLO-RAHMAN DYNAMICS

##### A. Equations of Motion

An implementation of Langevin Dynamics in a fully flexible simulations cell follows from the Nosé-Hoover thermostatted Parrinello-Rahman scheme of Martyna, Tobias and Klein [14] after removing the Nosé-Hoover chains and converting to Langevin equations in the momenta:

$$\dot{\mathbf{r}}_i = \frac{\mathbf{p}_i}{m_i} + \frac{\mathbf{p}_g}{W_g} \mathbf{r}_i \quad (23a)$$

$$\dot{\mathbf{p}}_i = -\nabla_{\mathbf{r}_i} \Phi(\mathbf{r}^N, \mathbf{h}) - \frac{\mathbf{p}_g}{W_g} \mathbf{p}_i - \left(\frac{1}{N_f}\right) \frac{\text{Tr}[\mathbf{p}_g]}{W_g} \mathbf{p}_i - \gamma \mathbf{p}_i + \mathbf{R}_i \quad (23b)$$

$$\dot{\mathbf{h}} = \frac{\mathbf{p}_g \mathbf{h}}{W_g} \quad (23c)$$

$$\dot{\mathbf{p}}_g = \mathcal{V}(\mathbf{X} - P_{ext}\mathbf{I}) + \left[ \frac{1}{N_f} \sum_{i=1}^N \frac{\mathbf{p}_i^2}{m_i} \right] \mathbf{I} - \gamma_p \mathbf{p}_g + \mathbf{R}_p \quad (23d)$$

where the tensor  $\mathbf{X}$  is given by

$$\mathbf{X}_{\alpha,\beta} = \frac{1}{\mathcal{V}} \left[ \sum_{i=1}^N \frac{(\mathbf{p}_i)_\alpha (\mathbf{p}_i)_\beta}{m_i} + (\mathbf{r}_i)_\alpha (\mathbf{f}_i)_\beta - (\phi' \mathbf{h}^T)_{\alpha,\beta} \right] \\ (\phi')_{\alpha,\beta} = \frac{\partial \phi(\mathbf{r}^N, \mathbf{h})}{\partial (\mathbf{h})_{\alpha,\beta}} \quad (24)$$

As before, we draw the random forces  $\mathbf{R}_i$  from the same distribution as in the NVT case. Each component of the barostat buffeting tensor  $\mathbf{R}_p$  is drawn from a Gaussian distribution on unit mean and zero variance scaled by

$$\sqrt{\frac{2k_B W_g \gamma_p}{\Delta t}}. \quad (25)$$

where  $W_g$  is set by the barostatic frequency  $\omega_b$  according to

$$W_g = (N_f + d)k_B T / d\omega_b^2. \quad (26)$$

These equations can be evolved using an analogous integration scheme to that described for the isotropic case in section III C. Appropriate frequencies for the thermostat and barostat are also chosen in the same way as for the isotropic scheme.

##### B. Analysis

Equations 23a to 23d conserve the quantity

$$H' = \mathcal{H}(\mathbf{r}^N, \mathbf{p}^N) + \frac{1}{2W_g} \text{Tr}[\mathbf{p}_g \mathbf{p}_g^T] + P_{ext} \det[\mathbf{h}] \quad (27)$$

in the limit of zero friction (the pure Parrinello-Rahman system). As in the Hoover case, this is not a true Hamiltonian. The system of equations cannot be derived from equation 27 via Hamiltons equations. The phase space analysis therefore requires the tools of Tuckerman *et al* [4, 5], and merits more attention than in the Hoover case.

The compressibility  $\kappa$  of equations 23a to 23d in the zero friction limit determines the uniformity of the background system in which we wish to perform Langevin Dynamics. For this system

$$\kappa = \sum_{i=1}^N \nabla_{\mathbf{r}_i} \cdot \mathbf{r}_i + \sum_{i=1}^N \nabla_{\mathbf{p}_i} \cdot \mathbf{p}_i \\ + \sum_{\alpha=1}^d \sum_{\beta=1}^d \frac{\partial (\dot{\mathbf{h}})_{\alpha,\beta}}{\partial (\mathbf{h})_{\alpha,\beta}} + \sum_{\alpha=1}^d \sum_{\beta=1}^d \frac{\partial (\dot{\mathbf{p}}_g)_{\alpha,\beta}}{\partial (\mathbf{p}_g)_{\alpha,\beta}}, \quad (28)$$

which can be simplified to

$$\begin{aligned}\kappa &= (d-1)\text{Tr}[\mathbf{p}_g]/W - d\text{Tr}[\mathbf{p}_g]/W + d\text{Tr}[\mathbf{p}_g]/W + 0 \\ &= (d-1)\text{Tr}[\mathbf{p}_g]/W.\end{aligned}\quad (29)$$

We then identify the scalar strain rate  $\dot{\epsilon}$  as  $\text{Tr}[\mathbf{p}_g]/Wd$ , and can therefore construct the Jacobian of the co-ordinate transform which takes the system from  $t=0$  to  $t'=t$  as

$$J(t;0) = \exp\left(\int_0^t d(d-1)\dot{\epsilon} dt'\right), \quad (30)$$

and hence the phase space metric is

$$\sqrt{g(t;0)} = \frac{V_{ref}^{d-1}}{\mathcal{V}^{d-1}} \propto \frac{1}{\det(\mathbf{h})^{d-1}}, \quad (31)$$

where  $V_{ref}$  is the volume of the cell to which the strain is referenced. We therefore expect the correctly ther-

mostatted probability distribution in the extended phase space to be

$$\rho(\mathbf{r}^N, \mathbf{p}^N, \mathbf{h}, \mathbf{p}_g) \propto \exp[-H'/k_B T] \det[\mathbf{h}]^{-2}. \quad (32)$$

Integration of this over the  $d^2$  components of the strain momentum tensor  $\mathbf{p}_g$  again yields a constant, yielding

$$\rho(\mathbf{r}^N, \mathbf{p}^N, \mathbf{h}) \propto \exp[-(\mathcal{H} + P_{ext} \det[\mathbf{h}])/k_B T] \det[\mathbf{h}]^{-2}, \quad (33)$$

which has previously been identified [14] as the correct phase space distribution for the isobaric-isothermal ensemble with a fully flexible cell. We can therefore conclude that the Parrinello-Rahman Langevin dynamics scheme will be capable of correctly sampling this ensemble if equation 32 is a solution of the following Fokker-Planck equation obtained from equations 23a to 23d.

$$\begin{aligned}\frac{\partial \rho}{\partial t} &+ \sum_{i=1}^N \left\{ \left( \frac{\mathbf{p}_i}{m_i} + \frac{\mathbf{p}_g}{W_g} \mathbf{r}_i \right) \cdot \nabla_{\mathbf{r}_i} \rho + \left[ \mathbf{f}_i - \frac{\mathbf{p}_g}{W_g} \mathbf{p}_i - \left( \frac{1}{N_f} \right) \frac{\text{Tr}[\mathbf{p}_g]}{W_g} \mathbf{p}_i \right] \cdot \nabla_{\mathbf{p}_i} \rho \right\} \\ &+ \sum_{\alpha, \beta} \left\{ \left[ (\mathbf{X}_{\alpha\beta} - P_{ext} \delta_{\alpha\beta}) \det[\mathbf{h}] + \frac{1}{N_f} \sum_{i=1}^N \frac{\mathbf{p}_i^2}{m_i} \right] \frac{\partial \rho}{\partial (p_g)_{\alpha\beta}} + \left( \frac{\mathbf{p}_g \mathbf{h}}{W_g} \right)_{\alpha\beta} \frac{\partial \rho}{\partial (h)_{\alpha\beta}} \right\} \\ &= \gamma \sum_{i=1}^N \nabla_{\mathbf{p}_i} \cdot [\mathbf{p}_i \rho + m k_B T \nabla_{\mathbf{p}_i} \rho] + \gamma_p \sum_{\alpha, \beta} \frac{\partial}{\partial (p_g)_{\alpha\beta}} \left[ (p_g)_{\alpha\beta} \rho + W_g k_B T \frac{\partial \rho}{\partial (p_g)_{\alpha\beta}} \right].\end{aligned}\quad (34)$$

Analysis of the LHS yields zero. This is equivalent to the statement that the extended phase space obeys the generalised Liouville theorem in the limit of zero friction. The background system in which the Langevin dynamics simulation is conducted therefore has a constant, but non-uniform probability density which conserves equation 27.

This introduces the possibility that the Stokes-Einstein relation which we have used to balance the diffusion and friction terms in our Langevin equations may be invalid. When balancing these two terms (equation 3) we have implicitly assumed that the background probability density is flat, i.e. no background probability gradients. Fortunately all such gradients in the Parrinello-Rahman system are perpendicular to the particle momentum axes and hence the first term on the RHS of equation 34 represents balanced Langevin dynamics and is zero.

The second term of the RHS is however not zero. The background probability gradients do effect the balance of diffusion and friction for the Langevin equation in the

cell momentum. In the case where symmetrised pressure and cell buffetting tensors have been used to eliminate cell rotations, the imbalance is small and proportional to  $\gamma_p$ . Purists may therefore wish to remove the cell thermostat. In practise, the effect makes little difference in real simulations and so it is possible to use a finite  $\gamma_p$  to aid equilibration. Any benefits this introduces are however, likely to be small.

## V. EXAMPLES

### A. Lennard-Jones Argon

In this section we will follow through the steps of conducting an isotropic constant pressure Langevin dynamics simulation for high pressure liquid argon modelled using the familiar Lennard-Jones potential. In particular we will investigate the temperature and density fluctua-

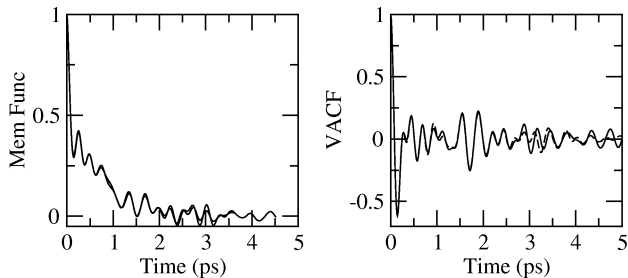


FIG. 3: NVE (solid line) and NVT Nosé-Hoover (dashed line) VACF and memory function for Lennard-Jones argon at 80 K 3.36 GPa. These are computed from 256 atom trajectories using the autoregressive model of Kneller and Hinsen [23] (order 150) as implemented in the nMoldyn program [24].

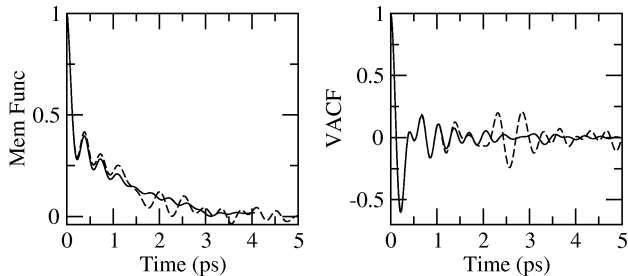


FIG. 4: VACF and memory function for 4000 (solid-line) and 256 (dashed-line) Lennard-Jones argon NVT Nosé-Hoover simulations at 80 K and equal densities equivalent to 3.36 GPa.

tions of this system at 80 K, 3.36 GPa. This corresponds to a total energy of approximately 0.105 Hartree for 256 atoms occupying a cubic cell of dimension 19.05 Å.

We will also simulate a solid argon system using the Parrinello-Rahman based scheme and again investigate the quality of the fluctuations.

### 1. Step 1

First we obtain a memory function relevant to this state point by conducting an NVE simulation (energy 0.105 Hartree, volume  $(19.05 \text{ Å})^3$ ).

The resulting VACF and memory functions are shown in figure 3. We also plot the equivalent functions calculated from a Nosé-Hoover NVT simulation to ensure our calculated value of  $\gamma$  will be appropriate for a system coupled to a heat bath. As can be seen the two memory functions are near identical in this case. Numerical integration under the memory function reveals an appropriate value for  $\gamma$  of  $2.41 \times 10^{-3} \text{ rad fs}^{-1}$ .

Note that in order to ensure that the value of  $\gamma$  chosen is truly representative of a bulk liquid system, we must ensure that the simulation used in its identification covers a length scale larger than that of any spacial correlations. For the purposes of this example we therefore also conduct a simulation using 4000 atoms and compute

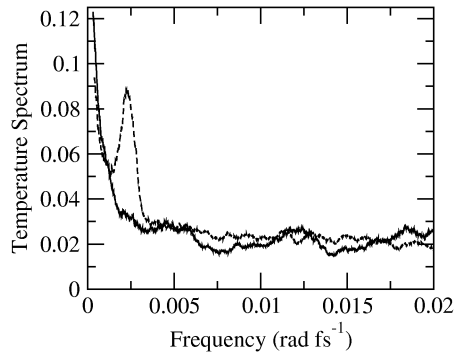


FIG. 5: NVT (solid line) and NPT (dashed line) Langevin dynamics temperature Fourier transforms for the Lennard-Jones system at 80 K 3.36 GPa. The barostat frequency is chosen so as to only affect the low frequency components introduced by the thermostat, and not the higher frequency components characteristic of the liquid itself.

a memory function. The result is shown in figure 4 and indicates that our value of  $\gamma$  is suitable.

### 2. Step 2

We now conduct an NVT Langevin dynamics simulation using the optimally identified value of  $\gamma$  as described in section II. This allows a temperature spectrum to be calculated, providing a criterion for choosing a barostatic timescale. A run of 1638400 time-s.ps was performed in this case to provide a suitably illustrative example, however much shorter runs can be used in practise. As this system is liquid, we do not expect any significant features in the spectrum as confirmed in figure 5, and we therefore choose the barostat to operate in low frequency region below the influence of the thermostat i.e.  $\omega_b = 2 \times 10^{-4} \text{ rad fs}^{-1}$ .

### 3. Step 3

With suitable values of  $\omega_p$  and  $\omega_b$  identified, a reliable NPT simulation can be conducted. We have now also identified the timescales associated with the problem and can safely increase the calculation time-step from 1.2 to 9.6 fs. Using these parameters the system is equilibrated for 50,000  $\Delta t$  and then sampled every 10 time-s.ps for a further 500,000. The resulting temperature and volume distributions are shown in figure 6.

### 4. Solid Argon with Full Cell Fluctuations

To demonstrate the ability of the Langevin-Parrinello-Rahman (LPR) scheme to produce equally accurate temperature and volume sample distributions, we have also conducted simulations at 20 K, 67.6 MPa where argon is



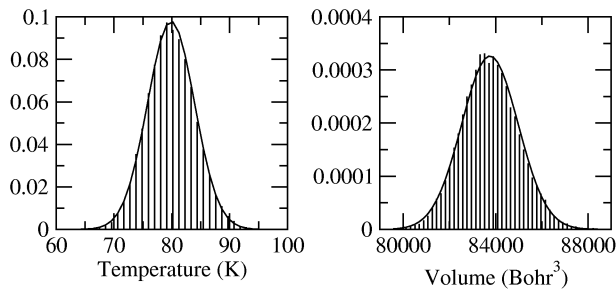


FIG. 6: Temperature and volume sample distributions calculated from Langevin-Hoover simulation compared to exact canonical cases for the Lennard-Jones argon system at 80 K 3.36 GPa. The compressibility required to calculate the ideal volume distribution was obtained from an earlier Nosé-Hoover based NPT calculation.

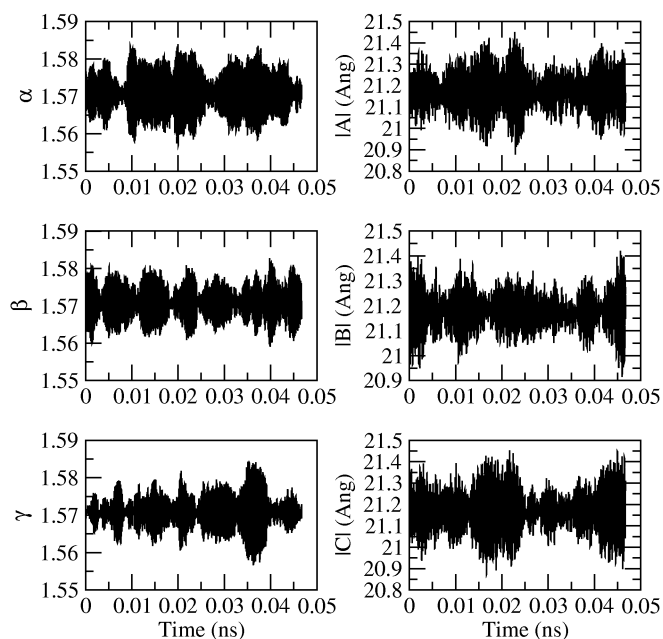


FIG. 7: Evolution of simulation cell during the 256 atom cubic cell LPR simulation of argon at 20 K 67.6 MPa.

a stable solid. Again memory functions were calculated from appropriate NVE and NVT simulations, and an appropriate frequency for the barostat was identified from the temperature spectrum as above. This process revealed suitable parameters of  $\omega_p = 1.33 \times 10^{-3} \text{ rad fs}^{-1}$  and  $\omega_w = 4.17 \times 10^{-5} \text{ rad fs}^{-1}$ .

These values were used in a simulation of a cubic cell of FCC argon containing 256 atoms. This system was equilibrated for 20,000  $\Delta t$  and then sampled every 10  $\Delta t$  for a further 750,000. A time-step of 9.6 fs was used. The resulting evolution of cell vectors is shown in figure 7, and the calculated distribution of temperature and volume samples is shown in figure 8. As with the liquid simulations using the isotropic algorithm, the distributions are of a very high quality.

## B. *Ab-initio* Silicon

In this section we will use the LPR scheme for the more realistic application of simulating silicon. We will first use the semi-empirical potential of Tersoff [25] to obtain an approximate memory function for crystalline silicon at room temperature and pressure. We will then use this memory function to choose parameters for a smaller silicon system using the LPR implementation in the *ab-initio* plane wave DFT code CASTEP [1].

### 1. Step 1

Again we perform both NVE and NVT runs with 216 atoms at the temperature and pressure of interest (using the Tersoff potential) in order to obtain a memory function characteristic of the system in question. These are shown in figure 9. A time-step of  $\Delta t = 2.0 \text{ fs}$  was used for a total run of 20,000  $\Delta t$  sampling every 4 time-s.ps after an initial equilibration period of 10,000  $\Delta t$ . The system was initialised with the expected equilibrium diamond structure.

Integration over the memory function yields a suitable thermostat frequency of  $3.05 \times 10^{-4} \text{ rad fs}^{-1}$ . This corresponds to a thermostat period of 20.81 ps.

For interest, we also compute a memory function for a Nosé-Hoover NVT simulation at the same state point using CASTEP. This was calculated for an eight atom cell using a cut-off energy of 160 eV and a time-step of 8 fs. The ultra-soft pseudo-potential method was used. The Brillouin zone was sampled at 4 k-points using the Monkhorst-Pack method, and the exchange and correlation functional was approximated using the LDA. The result is shown in figure 10. Although we expect this memory function to be subject to significant finite-size effects, the thermostat period obtained from this memory function is 16.95 ps, similar to that obtained from the larger system.

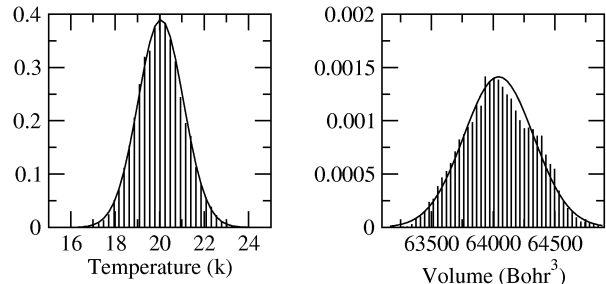


FIG. 8: Temperature and volume sample distributions of solid FCC argon at 20 K 67.6 MPa calculated using the LPR scheme. Exact canonical distributions are shown as solid lines.

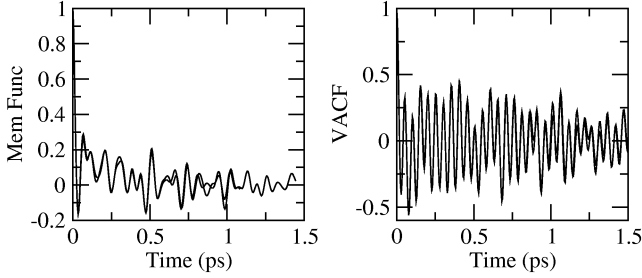


FIG. 9: NVE (solid line) and NVT (dashed line) VACF and memory function for the 216 silicon atom system modelled with the Tersoff potential at room temperature and atmospheric pressure.

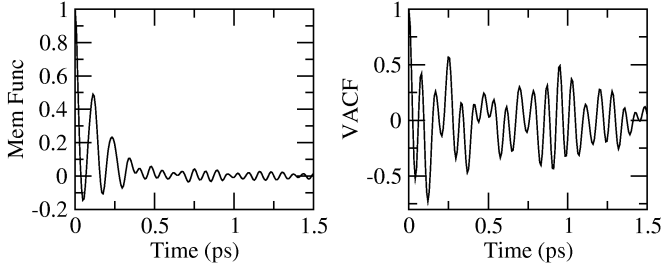


FIG. 10: Memory function and VACF calculated from the 8-atom *ab-initio* simulation of silicon at room temperature and pressure. These are expected to exhibit severe finite size effects, but are similar to those obtained from the Tersoff potential in figure 9.

### 2. Step 2

An NVT Langevin dynamics simulation at the required temperature and pressure (using the Tersoff potential) of 163,840  $\Delta t$  sampled every 10  $\Delta t$  yields the temperature spectrum shown in figure 11. For this example we use a value of  $\omega_b$  set to  $3.5 \times 10^{-3} \text{ rad fs}^{-1}$  which is well separated from the dominant frequencies and a few times smaller than that of the thermostat. The temperature profile for a NPT run at this value of  $\omega_b$  is also shown in figure 11, indicating that the choice is appropriate.

### 3. Step 3

With appropriate thermostat and barostat timescales obtained from the classical potential, we now perform the *ab-initio* LPR simulation. Again we use 4 k-points and a plane wave cut-off of 160 eV. The system was initialised in the ideal BC8 structure (cell parameter 5.75 Å) with random velocities, and equilibrated for 8,500  $\Delta t$ . The system was then sampled at a further 6,200 s.p.s. This represents a relatively simple simulation, requiring modest CPU time.

The resulting cell evolution is shown in figure 12. We also calculate the distribution of temperature and volume samples as shown in figure 13. For such a small simula-

tion, we do not expect exact fits to canonical distribution functions, however the plots indicate convergence toward the ideal results as demonstrated for argon above.

## VI. DISCUSSION

The results presented in the previous section have demonstrated that Langevin-Hoover and Langevin-Parrinello-Rahman schemes are capable of producing canonical fluctuations from which ensemble specific thermodynamic quantities can be calculated. Clearly the choice of parameters is important.

In this paper we have calculated optimal damping coefficients (and hence thermostat frequencies  $\omega_p$ ) for the stochastic component of the dynamics by computing a memory function for our example simulations. While this has provided optimal sampling efficiency, it has also complicated the choice of the barostat frequency  $\omega_b$ . We have stated earlier that the barostat frequency should be smaller than, but close to that of the simulated particles. This allows the particle motions to modulate the volume oscillation and hence generate canonical fluctuations. Too low a barostat frequency, and its motion becomes decoupled from the rest of the simulation, resulting in an undesirable slow harmonic oscillation of the volume. We also require the thermostat frequency  $\omega_p$  to be significantly higher than the barostat frequency  $\omega_b$ . This prevents disruption of the thermostatic process by the cell motion.

As we have chosen our Langevin friction co-efficient  $\gamma$  to be characteristic of the particle motions,  $\omega_p$  will be close to the particle frequency  $\omega$ . We also require  $\omega_b$  to be close to  $\omega$  but well separated from  $\omega_p$ . The choice of an optimal friction co-efficient therefore introduces an apparent conflict in the choice of barostat parameter. We have shown above in section III D that this issue can be

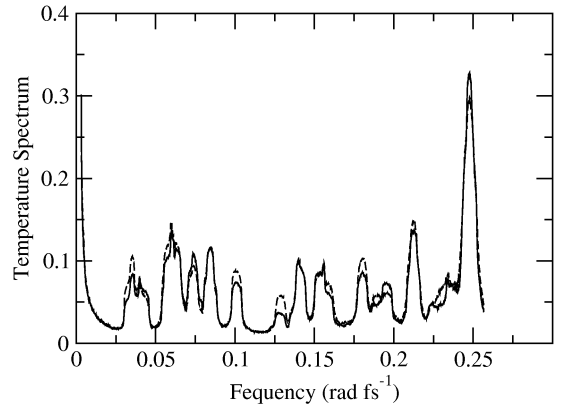


FIG. 11: NVT (solid line) and NPT (dashed line) Langevin dynamics temperature Fourier transforms for the 216 atom silicon system modelled using the Tersoff potential. The barostat frequency has been chosen to avoid disruption of the natural components and hence the two profiles are similar.

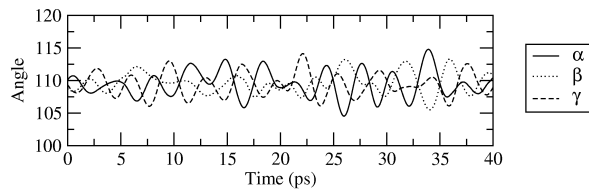


FIG. 12: Evolution of cell angles during the 8 atom *ab-initio* LPR simulation.

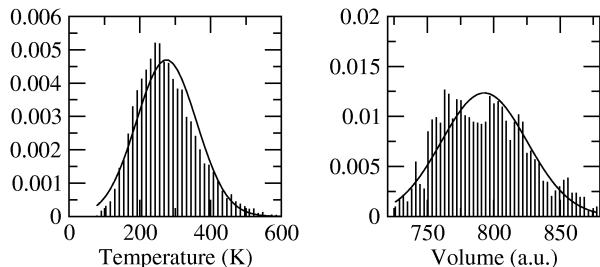


FIG. 13: Distribution of temperature and volume samples during the 8 atom *ab-initio* LPR simulation. The solid lines are the calculated canonical bulk values for comparison. although it should be noted that both distributions *should* differ from the bulk cases which are derived for large  $N$ .

overcome by use of the temperature spectrum in carefully choosing the barostat parameter.

It is important to note that this is not always the case in practise. The optimal friction co-efficient identified from the memory function represents the boundary between performing molecular dynamics with a ‘Langevin thermostat’ (i.e. low  $\omega_p$  with similar correlation times and sampling efficiencies as a Nosé-style thermostat for chaotic systems) and performing a ‘true Langevin dynamics’ simulation where the stochastic components dominate and are guided by the particle interaction forces (high  $\omega_p$ ). For the purposes of sampling an isothermal ensemble, a small conservative choice of  $\omega_p$  will also produce canonical temperature fluctuations, but on a longer timescale. The value calculated from the memory function therefore represents the best compromise between efficiency and preservation of accuracy in short-term dynamics.

As a conservative rule of thumb,  $\omega_p$  can be set a few tens of times smaller than the particle frequency  $\omega$ , and  $\omega_b$  can be chosen a few times smaller again. This allows canonical simulations in either the isotropic or fully flexible cell NPT ensemble to be generated with ease, albeit with a reduced sampling efficiency due to weaker modulation of the volume oscillation. A compromise must therefore be reached between the computational expense of computing optimal parameters, and statistical efficiency

in the simulation itself.

This stochastic approach bypasses any concerns about possible ‘hidden’ conservation laws [5] in Nosé style schemes which can incorrectly restrict trajectories and lead to incorrect ensemble averages. This effect in a simple harmonic potential is well documented (although still not entirely understood) and is generally thought to be ignorable in practical simulations. Often a chain of thermostats is used to break any unphysical conservation laws, however this process takes place on a longer timescale than in a stochastic thermostating scheme - an important consideration in *ab-initio* dynamics.

Solids at low temperature are essentially harmonic, as are the forces used to ‘connect’ different realisations in imaginary time during path-integral molecular dynamics simulations. We therefore suggest that the isobaric-isothermal sampling schemes presented here are a desirable alternative to traditional deterministic schemes for many applications.

## VII. CONCLUSIONS

We have shown that performing Langevin dynamics within constant pressure extended systems is a valid method for simulating the equilibrium isobaric-isothermal ensemble. An analysis of the phase space in these simulations has been presented, which shows that the correct distribution of probability is generated, provided the non-Hamiltonian nature of the extended system is accounted for.

We have derived a suitable integration scheme, analogous to the Velocity-Verlet scheme, which allows reversible integration of trajectories in the zero friction limit, and eliminates long term drift of the conserved quantity in the extended system when the stochastic component is introduced.

Suitable distributions of temperature and volume samples can be achieved provided a little care is taken in choosing parameters. Methods for identification of optimal values of these parameters have been presented, We have also discussed less stringent criteria for choosing parameters in the case where computing a memory function or an accurate NVT temperature spectrum is computationally prohibitive.

We consider this scheme to be a desirable alternative to extended system NPT schemes with Nosé-style thermostats, in particular for small or approximately harmonic systems, where deterministic schemes can suffer from unexpected coupling to the particle sub-system leading to incorrect trajectories, and consequent thermodynamics averages.

- [2] S. Nosé, J. Chem. Phys. **81**, 511 (1984).
- [3] W. G. Hoover, Phys. Rev. A **31**, 1695 (1985).
- [4] M. E. Tuckerman, C. J. Mundy, and G. J. Martyna, Europhys. Lett. **45**, 149 (1999).
- [5] M. E. Tuckerman, Y. Liu, G. Ciccotti, and G. J. Martyna, J. Chem. Phys. **115**, 1678 (2001).
- [6] S. D. Bond, B. J. Leimkuhler, and B. B. Laird, J. Comput. Phys. **151**, 114 (1999).
- [7] G. J. Martyna, M. L. Klein, and M. Tuckerman, J. Chem. Phys. **97**, 2635 (1992).
- [8] A. C. Branka, M. Kowalik, and K. W. Wojciechowski, J. Chem. Phys. **119**, 1929 (2003).
- [9] B. B. Laird and B. J. Leimkuhler, Phys. Rev. E. **68**, 016704 (2003).
- [10] H. C. Andersen, J. Chem. Phys. p. 2384 (1980).
- [11] W. G. Hoover, Phys. Rev. A **34**, 2499 (1986).
- [12] M. Parrinello and A. Rahman, Phys. Rev. Lett. p. 1196 (1980).
- [13] M. Parrinello and A. Rahman, J. Appl. Phys. **52**, 7182 (1981).
- [14] G. J. Martyna, J. T. Tobias, and M. L. Klein, J. Chem. Phys. **101**, 4177 (1994).
- [15] J. B. Sturgeon and B. B. Laird, J. Chem. Phys. **112**, 3474 (2000).
- [16] A. Kolb and B. Dunweg, J. Chem. Phys. **111**, 4453 (1999).
- [17] M. Tuckerman, B. J. Berne, and G. J. Martyna, J. Chem. Phys. **97**, 1990 (1992).
- [18] S. Chandrasekhar, Rev. Mod. Phys. **15**, 1 (1943).
- [19] W. G. Hoover, K. Aoki, C. G. Hoover, and S. V. De Groot, Physica D **187**, 253 (2004).
- [20] M. P. Allen and D. J. Tildesley, *Computer Simulation of Liquids* (Oxford University Press, New York, 1987).
- [21] R. L. Stratonovich, *Topics in the Theory of Random Noise II* (Gordon and Breach, New York, 1967).
- [22] G. J. Martyna, M. E. Tuckerman, D. J. Tobias, and M. L. Klein, Mol. Phys. **87**, 1117 (1996).
- [23] G. R. Kneller and K. Hinsen, J. Chem. Phys. **115**, 11097 (2001).
- [24] T. Rog, K. Murzyn, K. Hinsen, and G. R. Kneller, J. Comput. Chem. **24**, 657 (2003).
- [25] J. Tersoff, Phys. Rev. B **39**, 5566 (1989).